Effect of Nitriding-Quenching and Carburizing-Quenching Processes on the Wear Resistance of the Sintered Pure Iron

KOZIN, Muhammad
Graduate School of Engineering, Kyushu University

KUSAKABE, Keisuke
Undergraduate School of Engineering, Kyushu University

ARAMAKI, Masatoshi
Department of Materials Science and Engineering, Kyushu University

YAMADA, Naoya
Nihon Techno, Co., Ltd.

他

出版情報：粉体および粉末冶金. 67 (4), pp.173-181, 2020-04-15. 粉体粉末冶金協会
バージョン：

J. Jpn. Soc. Powder Powder Metallurgy, **67** (2020) 173-181
https://doi.org/10.2497/jjspm.67.173

Paper

Effect of Nitriding-Quenching and Carburizing-Quenching Processes on the Wear Resistance of the Sintered Pure Iron

Muhammad KOZIN[1,2], Keisuke KUSAKABE[3], Masatoshi ARAMAKI[4], Naoya YAMADA[5], Satoshi OUE[4], Yukiko OZAKI[4]*, Osamu FURUKIMI[4] and Masaki TANAKA[4]

[1]Graduate School of Engineering, Kyushu University, 744 Motooka, Nishi-ku, Fukuoka 819-0395, Japan.
[2]Agency for the Assessment and Application of Technology, Jakarta 10340, Indonesia.
[3]Undergraduate School of Engineering, Kyushu University, 744 Motooka, Nishi-ku, Fukuoka 819-0395, Japan.
[4]Department of Materials Science and Engineering, Kyushu University, 744 Motooka, Nishi-ku, Fukuoka 819-0395, Japan.
[5]Nihon Techno, Co., Ltd., Saitama 349-0133, Japan.

Received December 6, 2019; Revised February 16, 2020; Accepted February 17, 2020

ABSTRACT

In the present study, we have examined the wear properties of the sintered pure iron subjected to two distinct heat treatments such as nitriding-quenching (NQ) and carburizing-quenching (CQ). Based on our current observations, the martensite layer was formed on the surface layer following each treatment, whereas the hardness of the NQ martensite was much higher than that of the CQ one. The wear of the CQ specimen was slightly smaller than that of the NQ martensite, despite the lower value of the initial hardness. Meanwhile, the hardness of the CQ surface after the sliding tests significantly elevated relative to the NQ surface resulting in the better wear resistance. EBSD analysis demonstrated that the plastic deformation on the CQ surface along the sliding direction. Furthermore, the micro area X-ray diffraction along the surface layer of the CQ surface showed that a small amount of the retained austeite which reduced locally during the test. Therefore, the CQ-treated surface showed the excellent wear resistivity due to the surface hardening by the stress-induced transformation of the retained austenite dispersed in the martensite, in addition to the strain hardening of the martensite itself. In contrast, the worn surface of the NQ specimen showed slight plastic deformations of the ferrite grains beneath the martensite layer, but not in the surface martensite layer. This deformation under the martensite layer was due to the hardness gap between inward and the heat-treated surface, and might contribute to form the concave profile on the sliding surface. Consequently, this study could demonstrate such the difference in the wear mechanisms between the CQ and the NQ specimens.

KEY WORDS

sintered pure iron, nitriding, carburizing, wear resistance, nano-indentation hardness

1 Introduction

The sintered iron and steel have been widely used in various applications such as automotive components[1-3], tool steels[4,5] and implant materials[6,7]. The widespread employment of the powder metallurgy process in many different applications is dependent on its ability to produce complex parts[3]. The powder metallurgy processing consists of the powder production, compaction and sintering process[8]. This process utilizes the metal powders as the raw materials and thus has a wide range of the material compositions, which makes it much more advantageous than the other processes[3]. However, most of the low-alloy sintered parts cannot be used as-sintered, especially for the certain applications requiring the highly mechanical properties[9]. Therefore, the subsequent treatment is necessary to enhance the mechanical properties of the sintered parts.

Many surface hardening processes of the wrought steel, such as carburizing-quenching (CQ) and carbo-nitriding-quenching (CNQ) have been developed to improve the wear resistance[10-13]. However, since these processes comprised of the carburizing conducted at the high temperatures[14-16], the dimensional changes often take place during the treatments. To override this serious problem, nitriding-quenching (NQ) treatment has recently been developed[15-18]. Different from CQ and CNQ, this treatment is performed under the lower temperature since the austenite phase of Fe-N system is stable under the lower temperature than that of Fe-C one. During this process, the steels are heated up to the austenitizing

* Corresponding author, E-mail: ozaki@zaiko.kyushu-u.ac.jp

temperature under NH_3 gas atmosphere followed by quenching. During the heating process, nitrogen atoms diffuse onto the steel surface, which is subsequently quenched to form the iron-nitrogen martensite phase. The hardened surface layer includes the iron-nitrogen martensite and the iron nitride compounds such as ε-$Fe_{2\sim3}N$ and γ'-Fe_4N phases[15-19]. Especially, the quenching from the austenitizing temperature in the single-phase austenite region produced the nitrogen martensite without any iron nitride[16-17].

We have previously described the effects of NQ conditions on the wear properties of the hot-rolled industrial pure iron[16]. According to our results, the heat-treated surface including the nitrogen martensite and the iron nitride compounds exhibited the higher wear resistance relative to the surface composed of the nitrogen martensite alone. Furthermore, the wear resistance of the hot-rolled industrial pure iron treated by CQ process was also examined. The carburized specimen, where the carbon martensite was formed in the surface layer, showed the similar level of the wear resistance to the former specimen treated by NQ process. These observations strongly indicate that both NQ and CQ processes effectively increase the wear resistance of the hot-rolled industrial pure iron. On the other hand, NQ process has not yet been applied to the sintered steel.

In this study, the wear behaviors of both NQ- and CQ- treated sintered irons were compared in order to confirm the possibility of NQ treatment to sintered steel.

2 Experimental procedures

2.1 Specimen preparation

The sintered pure iron used for the present study was produced from the atomized pure iron powder (JIP301A) with the indicated chemical composition (Table 1). Its thickness, width and length were of 10 mm, 10 mm and 55 mm, respectively. The powder was cold pressed and sintered at 1,403 K for 1.2 ks in H_2 gas atmosphere, resulting in the sintered product with a density of 7.05 Mg/m^3. The product was then sliced to form the specimens with 1.2 mm in thick, 10 mm in width and 10 mm in length. Their surfaces were ground using 1,000-grit emery paper before the nitriding or carburizing treatment. Schematic diagrams of the heat treatments were shown in Fig. 1. For NQ treatment, after holding at 1,033 K for 1.8 ks in N_2 gas atmosphere, the specimen was soaked under NH_3 gas atmosphere at 1,033 K for 3.6 ks and then oil quenched. Subsequently, the low-temperature tempering was performed at 443 K for 7.2 ks (Steel A). The N_2 and NH_3 flow rates upon the nitriding were set to 3.0 m^3/h and 0.24 m^3/h, respectively. For CQ treatment, after holding the specimen at 1,203 K for 0.6 ks in N_2 and for 1.2 ks in the evacuation, the carburizing was carried out at the carbon potential of 0.85% for 0.9 ks in C_2H_2-N_2 atmosphere (Fig. 1b). The specimen was held at 1,203 K for 0.9 ks and at 1,113 K for 1.8 ks in N_2 for the controlling carburized depth followed by the oil quenching. Subsequently, the low-temperature tempering was conducted at 443 K for 7.2 ks (Steel B). During the carburizing, C_2H_2 gas was introduced intermittently at 60 kPa by 32 x 10^{-3} m^3/pulse for 180 s to N_2 gas flow of 1.0 m^3/h. In addition, the sintered pure iron specimen, which was not subjected to any heat treatment (Steel C), was also prepared for the comparison.

Table 1 Chemical composition of the atomized pure iron powder JIP301A (mass%).

C	Si	Mn	P	S	O	Fe
0.002	0.01	0.17	0.011	0.007	0.153	Bal.

2.2 Observation of the microstructures

After the heat treatment, the specimens were sliced along C/N diffusion direction, and the cross-section was sequentially polished using the emery papers (#320 up to #2000), 3 μm and 1 μm of the diamond paste and the colloidal silica. After polishing, the argon ion milling (IM 3000, Hitachi) was applied for 5 min, and then the sample was etched using 3% nital solution. The microstructures were examined using the field emission scanning electron microscope (FE-SEM Ultra 55, Carl Zeiss) with the accelerating voltage of 5 kV. The crystal structures were analyzed by the electron backscatter diffraction (EBSD) installed on the scanning electron microscope (SU6600, Hitachi High-Technologies) with the accelerating voltage of 15 kV.

2.3 Hardness test

The hardness distribution of the specimens from the surface was measured by using the nano-indentation hardness tester (ENT-1100b, Elionix). Berkovich triangular pyramidal diamond indenter was employed with the applied load of 9.8 mN. The hardness was evaluated from the surface to the depth of 100 μm at intervals of

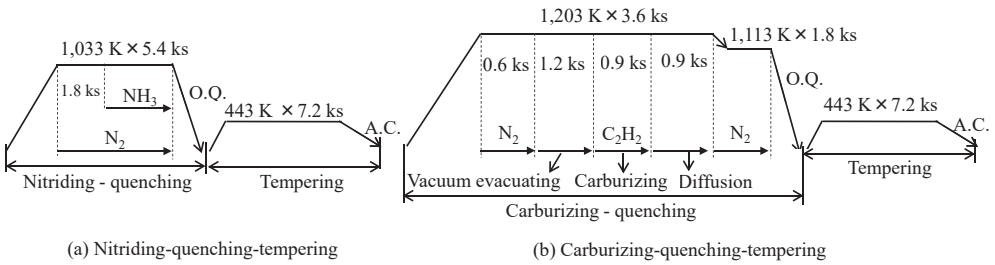

(a) Nitriding-quenching-tempering (b) Carburizing-quenching-tempering

Fig. 1 Schematic diagrams of the heat treatments: (a) nitriding-quenching-tempering and (b) carburizing-quenching-tempering.

5 μm. In addition, the hardness at the depth of 100–600 μm from the surface at interval of 10 μm was obtained in the same way.

2.4 Sliding test

To examine the wear characteristics, the sliding test was conducted using the "ring-on-plate" sliding test machine. This test was performed as described previously[16] and its schematic illustration was shown in Fig. 2. The inner and outer radii of the ring were 2 mm and 4 mm, respectively. The ring was made of JIS SKD 11 with the Vickers hardness of 670 HV. The sliding test was performed at the rotation speed of 100 rpm, which corresponded to the sliding speed of 31.4 mm/s under the contact pressure of 1.06 MPa without the lubrication. The total sliding distance was adjusted to 753.6 m. As the test was being performed, it was interrupted at the predetermined sliding distance, and the wear profile of the friction surface was measured using the laser scanning microscope (VK-9700, Keyence). The wear volume was obtained from the wear profiles[16]. The specific wear rate (W_s) was obtained from the wear volume (V), the test load (W) and the sliding distance (L) according to as follows:

$$W_s = \frac{V}{WL} \ [\mathrm{mm^3/J}] \quad (1)$$

Additionally, once the final sliding distance was achieved, the friction surfaces were observed using the field emission scanning electron microscope. To clarify the changes in the microstructure caused by the sliding test, EBSD analysis was performed on the cross-sectional surfaces of the specimen and the result was compared with the microstructure before the sliding test.

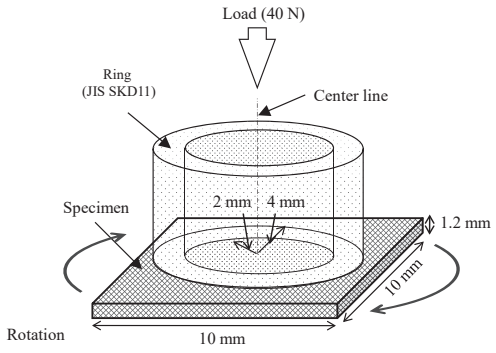

Fig. 2 Schematic illustration of the ring-on plate type sliding test.

2.5 X-ray diffraction in the surface layer

To measure the amount of the retained austenite in the surface layer before and after the sliding tests, the micro area X-ray diffraction was carried out at the depth within 300 μm along the surface layer of the section area of the specimens using Co-K_α X-ray beam of 300 μm diameter. The amount of the retained austenite was estimated by the ratio of the diffraction peak of γ-Fe (200) to α-Fe (211).

3 Results

3.1 Microstructures and the hardness of the nitrided and the carburized layers

Figs. 3a and 3b show SEM images of the cross-sectional surfaces of Steel A and Steel B. As shown in Fig. 3a, the nitride layer of Steel A was not uniform along the surface, whereas there existed the deep penetrations at some regions including pores. At the forefront of the nitride layer at a depth of 40 to 70 μm, nitride particles and non-nitride particles coexisted. This martensite layer found deeply inside, was produced during NQ treatment due to the pores which allowed the nitrogen diffusion around them. The nitrided layer of Steel A largely consisted of the nitrogen martensite. Since the nitriding temperature 1,033 K was detected in the austenite single-phase region, the compound layer (ε-$Fe_{2\sim3}N$ and γ'-Fe_4N phases) was not recognized after the quenching process in Steel A. In Steel B, the surface layer carburized at C.P. 0.85% consisted of the carbon martensite. However, the boundary of the carburized layer could not precisely be determined, because the carbon martensite phase existed in the whole part of the cross-sectional surface of Steel B (Fig. 3b). The surface hardened depth of Steel B was found to be much thicker than that of Steel A, raising a possibility that the higher carburizing temperature (1,203 K as compared to the nitriding temperature of 1,033 K) might cause the process to proceed with the faster and deeper carbon diffusion.

Nano-indentation hardness (H_{IT}) was measured inward from each surface of Steel A, B and C (Fig. 4). The H_{IT} of the specimen without the heat treatment (Steel C) was 1,770 N/mm^2, while those of Steel A and B with the heat treatment were increased up to 10,750 N/mm^2 and 7,700 N/mm^2, respectively, as measured at their outermost surfaces. While, the decrease in these values was

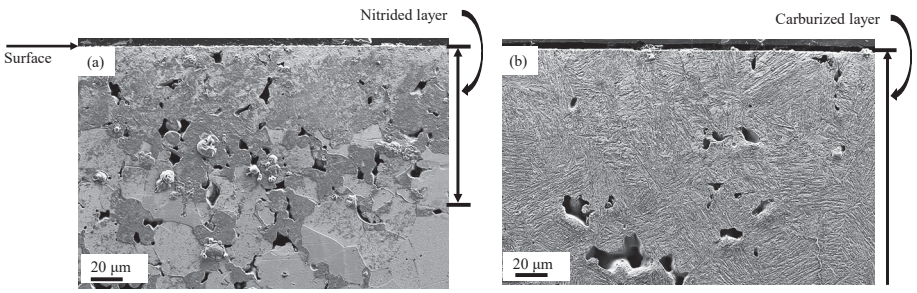

Fig. 3 SEM images of the cross-sectional surfaces of the specimens after the heat treatments: (a) the NQ-tempered Steel A and (b) the CQ-tempered Steel B.

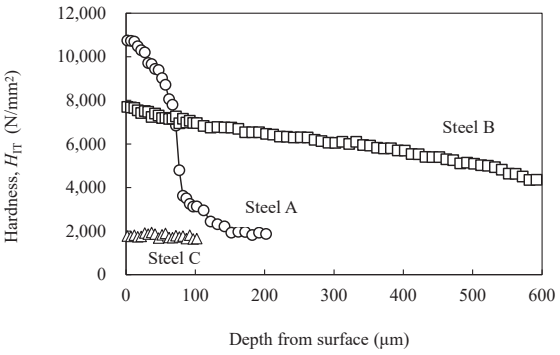

Fig. 4 Nano-indentation hardness profiles from the surface of the NQ-tempered Steel A, the CQ-tempered Steel B and the non-heat-treated Steel C.

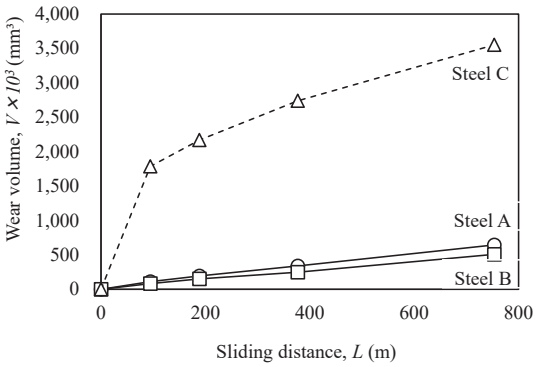

Fig. 6 Relationship between the wear volume and the sliding distance obtained by the sliding tests.

detectable in a depth-dependent manner. The depth measured on the hardened surface of Steel A was around 90 μm, whereas that of Steel B could not be precisely determined due to the still higher H_{IT} value at the depth of even half of the specimen's thickness (600 μm). Thus, it is likely that the depth of the hardened surface of Steel B is larger than 600 μm. Consistent with the microstructure analysis, these results indicate that the carburized layer of Steel B is much thicker than the nitrided layer of Steel A.

3.2 Sliding characteristics

Fig. 5 showed how the wear profile could be changed following the increase in the sliding distance. The wear depths of Steel A and B were relatively shallow compared to that of Steel C for each of the sliding distance. After 753.6 m sliding test, the maximum wear depths of Steel A, B and C were around 27 μm, 17 μm and 70 μm, respectively. In particular, the wear depth of Steel A was deeper than that of Steel B despite the much higher initial hardness of Steel A, compared to that of Steel B. This might be due to the strain hardening at the surface of Steel B during the sliding test, which led to the reduction in wear rate. Fig. 6 displayed the relationship between the wear volume and the sliding distance. As described previously[8], the wear phenomena were divided into two distinct stages such as the initial wear and the steady-state wear. As shown in Fig. 5, the initial wear was appeared to occur at 94.2 m sliding, after which the steady-state wear took place. For Steel C, the wear volume in the initial stage of the sliding test increased rapidly and then remained to increase at the relatively constant rate. On the other hand, the wear volumes of Steel A and B in the initial wear stages were extremely small and almost identical due to the presence of the nitrogen martensite and the carbon martensite layers. It is suggestive that these layers inhibit the activation of the surface degradation mechanisms.

Figs. 7a and 7b showed the specific wear rate calculated by eq. (1) of each specimen in the initial wear and the steady-state wear, respectively. In both wear stages, the wear rate of Steel C was much greater than those of Steel A and B. The specific wear rates of Steel A and B were comparable in the initial wear stage. Of note, Steel B exhibited the slightly lower wear rate than Steel A in the steady-state wear stage. These results indicate that both NQ- and

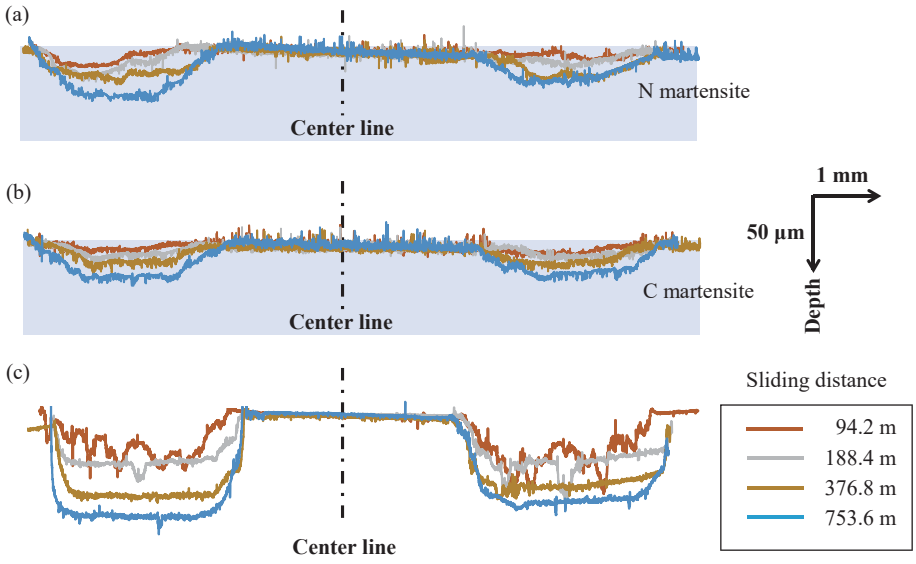

Fig. 5 Wear profile changes by the sliding distance: (a) the NQ-tempered Steel A, (b) the CQ-tempered Steel B, and (c) the non-heat-treated Steel C.

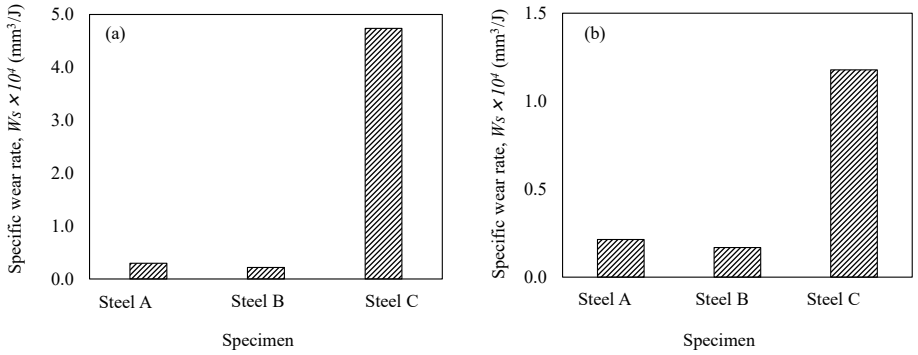

Fig. 7 Specific wear rates of each specimen obtained at the sliding distance: (a) 94.2 m and (b) 753.6 m.

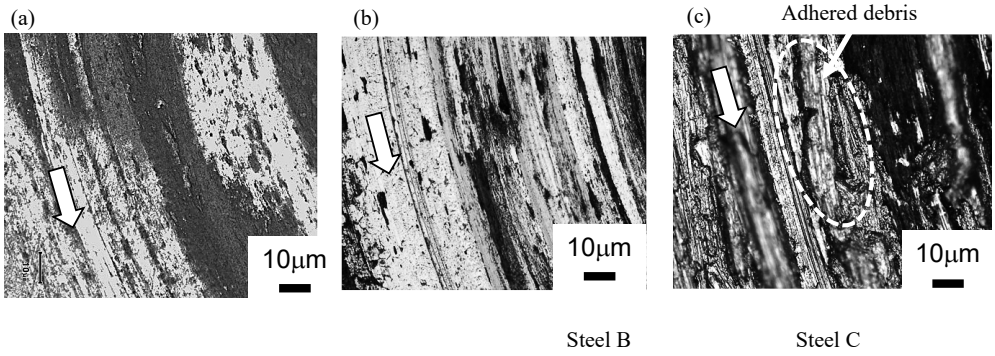

Fig. 8 SEM images of the worn track on the surfaces after 753.6 m sliding: (a) the NQ-tempered Steel A, (b) the CQ-tempered Steel B, and (c) the non-heat-treated Steel C.

CQ-treated surfaces can suppress the wear. In particular, the effect was significant in CQ specimen in the steady-state wear stage.

Figs. 8a-8c displayed SEM images of the worn track on the sliding surfaces of Steel A, B and C after 753.6 m sliding. Since the adhesive debris were rarely observed in Figs. 8a and 8b, the worn tracks on the heat-treated Steel A and B were abrasive wear like. In contrast, the stretched debris adhered on the worn track shown in Fig. 8c, suggesting that the worn track of Steel C might be adhesive wear like.

4 Discussion

4.1 Strain hardening on the sliding surfaces between NQ- and CQ-treated specimens

To examine the possible alteration of the surface hardness after the sliding test, the H_{IT} before and after the sliding tests from the surface up to the depth of 100 μm was measured (Fig. 9). After the sliding tests, the surfaces of Steel A, B and C shifted around 27 μm, 17 μm and 70 μm, respectively, due to the wear resulted from the sliding test. It is indicative that the hardness of Steel C before and after the sliding test is similar, regardless of the distance. In contrast, the surface hardnesses of Steel A and B were increased up to 11,300 N/mm^2 and 13,630 N/mm^2, respectively, after 753.6 m sliding. It is notable that the surface hardness of Steel B exhibited the marked increase relative to that before the sliding test (Fig. 9b). Collectively, it is likely that the increased surface hardness of Steel B after the sliding test is caused by the strain hardening induced by the shear deformation due to the shear force on the surface by the sliding with the counter material, leading to the wear resistance in Steel B at the steady-wear state (Fig. 5b) compared with Steel A where the shear deformation was not observed.

4.2 The microstructures of NQ- and CQ-treated specimens before and after the sliding tests

Fig. 10 displayed SEM images of the cross-sectional surfaces of Steel A, B and C after the sliding test (sliding distance of 753.6 m). Steel B and C exhibited the plastic flow and shear deformation in the layer where the pores stretched and squashed along the sliding direction (Figs. 10b and 10c). By contrast, the deformation was not detectable in Steel A, and the pores were not stretched in the area near the sliding surface of Steel A, although the shear stress should be concentrated around the pores. These observations indicate that the surface texture might be removed by the abrasive wear without any deformation.

To address the details of the plastic flow, the crystal structures of the cross-sectional surface of Steel A, B and C before and after the sliding tests were analyzed by EBSD (Fig. 11). In EBSD analysis, the color mapping was employed to measure the points at which confidence index (CI) was more than 0.1. Below this value (indicated in black), the indexing of the surface was impossible. Based on this criterion, the black part corresponded to the region in which the microstructure was considered very fine or included the high-density dislocations. Figs. 11a and 11d demonstrated IPF maps of the cross-sectional surfaces of Steel A before and after

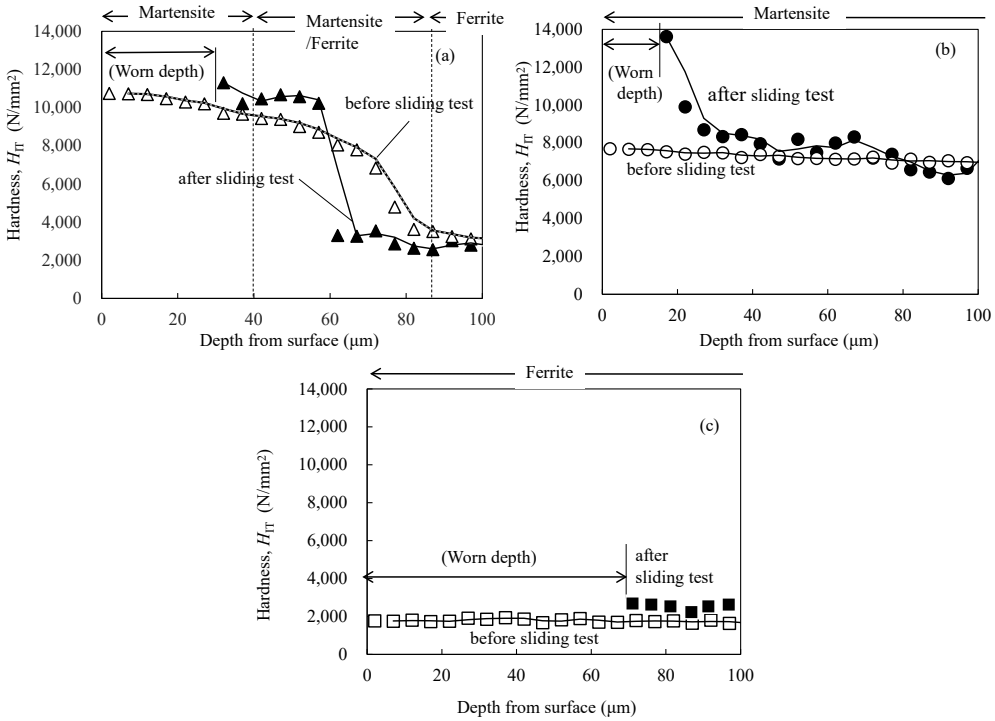

Fig. 9 Nano-indentation hardness profiles from the surface before and after the sliding tests at the distance of 753.6 m: (a) the NQ-tempered Steel A, (b) the CQ-tempered Steel B, and (c) the non-heat-treated Steel C.

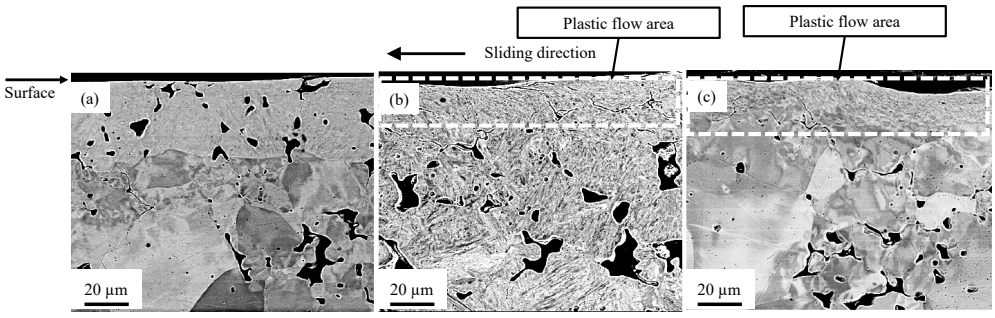

Fig. 10 SEM images of the cross-sectional surfaces after 753.6 m sliding tests: (a) the NQ-tempered Steel A, (b) the CQ-tempered Steel B, and (c) the non-heat-treated Steel C.

the sliding tests, respectively. Both nitrided layers showed the lath martensite structures (the nitrogen martensite), which were indexed as α-Fe (iron alpha). Comparing both figures, the nitrided layer slightly decreased by approximately 10 μm during sliding. Moreover, as shown in Fig. 11d, any deformation caused by the shear force was not observed near the sliding surface, and the strain was introduced to some ferrite grains adjacent to the surface martensite layer.

Fig. 11b displayed IPF images of the cross-sectional surface of Steel B before the sliding test. The surface layer was also the lath martensite, which was indexed as α-Fe (iron alpha). Under these conditions, the retained austenite phase was not confirmed. After the sliding test, the black area was detected in some parts of the surface layer, which did not exhibit the clear crystalline structure in the presence of the plastic flow caused by the shear force during the successive sliding (Fig. 11e).

The IPF maps of the cross-sectional surface of Steel C before and after the sliding test were shown in Figs. 11c and 11f, respectively. Fig. 11f displayed the extremely share deformation near the surface layer.

4.3 Wear mechanisms of the heat-treated sintered steels

4.3.1 NQ-treated specimen

The worn track of the NQ surface was abrasive like because the adhesive debris was not observed in Fig. 8a. However, comparing Figs. 11a and 11b, the thickness of the nitride martensite layer was not reduced by abrasion as much as the depth of the worn track (about 30 μm) estimated from the surface roughness profile shown in Fig. 5a. This result indicates the other factor forming the worn tracks. Focusing on the IPF map in Fig. 11d, the local strain can be seen not in the martensite layer itself, but in the ferrite grains adjacent to it. Therefore, it is considered that the compressive deformation of the ferrite layer under the surface

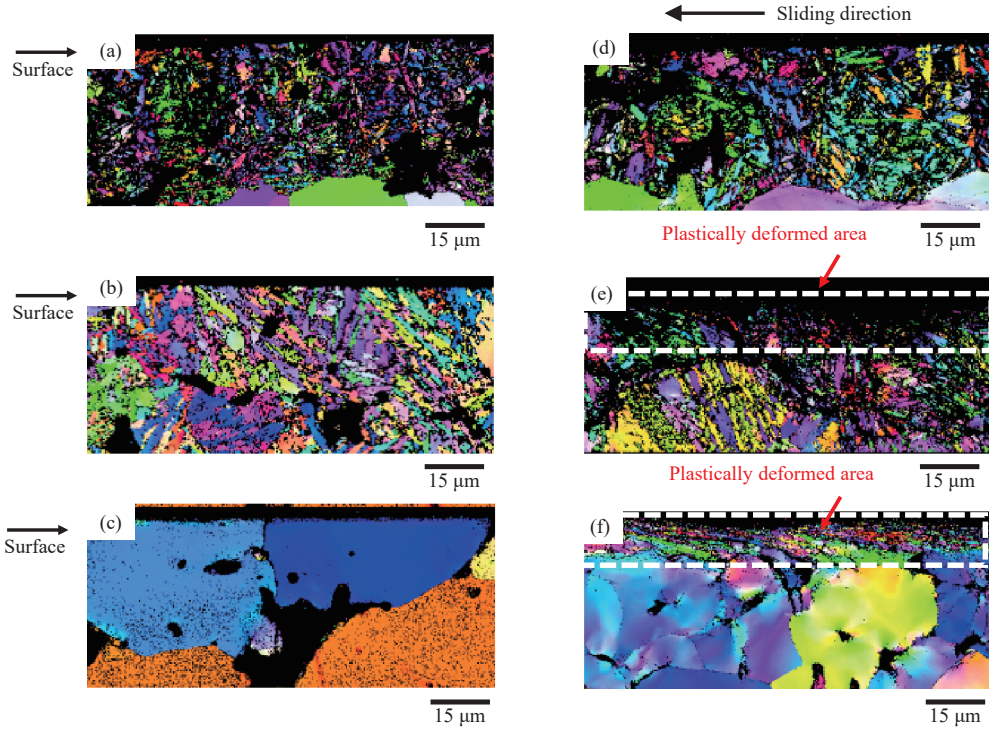

Fig. 11 IPF maps of the cross-sectional surfaces obtained from EBSD analysis before the sliding test: (a) the NQ-tempered Steel A, (b) the CQ-tempered Steel B, and (c) the non-heat-treated Steel C, and those of them after the sliding test at the distance of 753.6 m: (d) Steel A, (e) Steel B, and (f) Steel C.

martensite contributed to the formation of the concave profile of the sliding tracks in addition to the wear of the surface martensite layer itself. Such the deformation under the nitride martensite layer was considered to occur due to the hardness gap between inward and the surface. To elucidate this mechanisms, further studies should be required.

4.3.2 CQ-treated specimen

While the surfaces of both Steel B and C were similarly deformed, the significant increase in the hardness near the forefront of the worn surface was observed in Steel B but not in Steel C. In the low carbon steel, the strain hardening coefficient was decreased with the increase in C content[22]. Since the carburized surface of Steel B contained much more C than the non-carburized Steel C, the strain hardening coefficient of the former specimen should be lower than the latter one. It is possible that this significant hardening at the shear surface of Steel B is not only due to the strain hardening. While the retained austenite phase was not observed in EBSD analysis, the stress-induced transformation can occur easily in the carbon steel with >0.6% C[23]. To confirm the stress-induced transformation in the shear surface of Steel B with high C content, the amount of the retained austenite near the surface was measured using the micro area X-ray diffraction on the section area of the specimen after the sliding test (sliding distance of 753.6 m). Fig. 12 depicts the observed layers by the micro area X-ray diffraction. The specimen after the test was sliced along the line P-Q, and the XRD measurements were carried out along the layers of 300 μm wide beneath the both surfaces of the

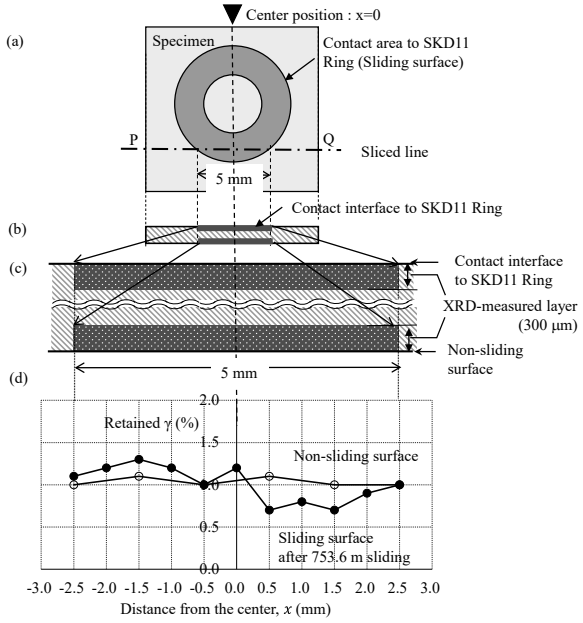

Fig. 12 The scheme of the micro area X-ray diffraction measurement to estimate the amounts of retained austenite in the surface layers of the CQ-tempered Steel B after the sliding test at the distance of 753.6 m: (a) top view of the specimen, (b) project view sliced along the line P-Q, (c) XRD-measured layers, along the worn surface sliding with the SKD11 ring (the upper side) and beneath the non-sliding surface (the bottom side) and (d) the amounts of retained austenite in the both layers.

specimen: one was the layer along the worn surface sliding with the SKD11 ring, and the other was the non-sliding surface on the opposite side. As shown in Fig. 12, about 1% of the retained

austenite was detected in each of the layers. Remarkably, the amount reduced locally in the layer beneath the sliding surface after the test. One of the previous works demonstrated the meaningful fact, through the TEM observation about a low carbon steel, that the retained austenite films of sub-micron thick were observed in the boundaries of lath boundaries, and they took place to hardening by the strain-induced transformation in addition to the strain hardening of the lath martensite itself in the primary stage of deformation[24]. Assuming such the fine retained austenite film at the lath martensite boundary in Steel B, it can be explained that the austenite films bring significant hardening by the stress-induced transformation. On the other hand, it should be noted that the retained austenite did not reduce in the left side of the sliding surface as shown in Fig. 12. It indicates that the plastic deformation of the specimen was not uniform because the specimen contacted ununiformly to the worn ring surface softer than the CQ-treated surface. To conclude, the CQ-treated surface showed the excellent wear resistivity concerning with the surface hardening due to the stress-induced transformation of the fine retained austenite in addition to the strain hardening of the lath martensite. Meanwhile, the effect of compressive deformation of the deep layer could not confirmed as mentioned in the CQ specimen, because the specimen was carburized throughout the thickness in the CQ treatment condition of this study. Therefore, to precisely discuss the wear mechanism compared with the NQ specimen, it is required that CQ-treated specimen with the surface-hardened layer depth as same as NQ-treated one in the future.

5 Conclusion

The sliding wear was compared between NQ- and CQ- treated sintered compacts of pure iron.

(1) The specific wear rate was much lower in both NQ- and CQ-treated materials compared to non-heat-treated specimen.

(2) The wear volume of the CQ-treated material was slightly less than that of the NQ-treated material, despite much lower initial hardness.

(3) No shear deformation was observed in the worn surface of the NQ-treated material. The nitrided surface formed into the concave surface due to the abrasive wear and a certain amount of the compressive deformation of the ferrite phase under the nitride martensite layer.

(4) At the surface layer of CQ material, the shear deformation near the worn surfaces was observed after the sliding test and at the same time the hardness was obviously increased. Since the retained austenite was decreased during the test, the wear resistivity might be improved concerning with the surface hardening due to the stress-induced transformation of the fine retained austenite in addition to the strain hardening of the lath martensite.

In conclusion, our present results demonstrated that the wear resistance of the steel is similarly improved by CQ and NQ processes, but there exist the different mechanisms behind the wear between them, which might be dependent on the strain hardening of the sliding surface and the hardness gap between inward and the heat-treated surface.

Acknowledgments

This work was supported in part by a Small and Medium-sized Enterprise Basic Act SMEs (SMEs) for the project “Development of method and its equipment for gas carburizing by adding acetylene gas (2016-2018)” from Kanto Bureau of Economy, Trade and Industry (METI-Kanto). The authors would like to thank JFE Steel Corporation for providing the specimens and the micro X-ray diffraction analysis as well as Nihon Techno, Co., Ltd. for the experimental supports.

References

1) G. B. Jang, M. D. Hur, S. S. Kang: J. Mater. Process. Technol., **100** (2000) 110-115.
2) T. F. Andrade, A. C. Zambon, C. H. C. Sena, A. G. Bida, J. R. Kavai: Mater. Sci. Forum, **727-728** (2012) 349-355.
3) A. Emamian: Mater. Sci. Appl., **3** (2012) 519-522.
4) K. J. Ducki, J. Jasiewicz, G. Junak, L. Wojtynek: Solid State Phenom., **226** (2015) 33-38.
5) M. Katarina, M. Peter, J. Dagmar: Applied Mechanics and Materials, **302** (2013) 269-274.
6) N. Kurgan, Y. Sun, B. Cicek, H. Ahlatci: Chin. Sci. Bull., **57** (2012) 1873-1878.
7) L. A. Dobrzański, A. D. Dobrzańska-Danikiewicz, A. Achtelik-Franczak, L. B. Dobrzański, E. Hajduczek, G. Matula: Intech (2017) 17-52.
8) M. Turkmen: Powder. Metall. Met. Ceram., **55** (2016) 164-171.
9) M. Askari, H. Khorsand, S. M. S. Aghamiri: J. Alloys Compd., **509** (2011) 6800-6805.
10) B. Selçuk, R. Ipek, M. B. Karamiş: J. Mater. Process. Technol., **141** (2003) 189-196.
11) E. Atik, U. Yunker, C. Meriç: Tribology Int., **36** (2003) 155-161.
12) M. B. Karamiş, R. Ipek: Appl. Surf. Sci., **119** (1997) 25-33.
13) M. L. Fares, A. Talhi, K. Chaoui, M. Z. Touhami: Surf. Eng., **27** (2011) 595-601.
14) C. Nan, D. O. Northwood, R. J. Bowers, X. Sun: Mater. Sci. Forum, **638-642** (2010) 829-834.
15) H. Katafuchi, M. Aramaki, N. Yamada, N. Chayapiwut, H. Kabasawa, O. Furukimi: Proceedings of European Conference on Heat Treatment and 21st IFHTSE Congress, Hans-Werner Zoch, Reinhold Schneider, and Thomas Lübben ed., Munich, International Federation for Heat Treatment and Surface Engineering, Arbeitsgemeinschaft Wärmbehandlung und

Werkstofftechnik e. V. (AWT), (2014) 467-470.
16) O. Furukimi, K. Katafuchi, M. Aramaki, M. Kozin, S. Oue, K. Yoshida, I. Narita, N. Yamada, M. Yamamoto: Mater. Trans. JIM, **57** (2016) 1587-1592.
17) N. Sato, M. Ojima, Y. Tomota, K. Inaba: Netsu Shori, **49** (2009) 304-307.
18) M. Chiba, G. Miyamoto, T. Furuhara: J. Japan Inst. Metals, **76** (2012) 256-264.
19) K. Tsukiyama, N. Nakada, T. Tsuchiyama, S. Takaki, Y. Tomota: Adv. Mat. Res., **922** (2014) 773-778.
20) T. Miyajima, Y. Iwai: Wear, **255** (2003) 606-616.
21) E. Fereiduni, S. S. G. Banadkouki: J. Alloys Compd., **577** (2013) 351-359.
22) C. S. Roberts: J. Metals, **5** (1953) 203-204.
23) M. Sekino, T. Fujishima: J. Jap. Inst. Metal. Mater., **39** (1975) 224-232.
24) S. Morito, T. Ohba, A. K. Das, T. Hayashi, M. Yoshida: Tetsu-to-Hagane, **96** (2012) 245-252.